symmetry

MDPI

Article

Probing a Hybrid Channel for the Dynamics of Non-Local Features

Atta ur Rahman [1], Macheng Yang [1], Sultan Mahmood Zangi [2,3] and Congfeng Qiao [1,4,*]

[1] School of Physical Sciences, University of Chinese Academy of Sciences, Yuquan Road 19A, Beijing 100049, China; attaphy57@mails.ucas.ac.cn (A.u.R.)
[2] Department of Physics, University of Okara, Okara 56300, Pakistan
[3] School of Physics and Astronomy, Yunnan University, Kunming 650500, China
[4] CAS Center for Excellence in Particle Physics, Beijing 100049, China
* Correspondence: qiaocf@ucas.ac.cn

Abstract: Effective information transmission is a central element in quantum information protocols, but the quest for optimal efficiency in channels with symmetrical characteristics remains a prominent challenge in quantum information science. In light of this challenge, we introduce a hybrid channel that encompasses thermal, magnetic, and local components, each simultaneously endowed with characteristics that enhance and diminish quantum correlations. To investigate the symmetry of this hybrid channel, we explored the quantum correlations of a simple two-qubit Heisenberg spin state, quantified using measures such as negativity, ℓ_1-norm coherence, entropic uncertainty, and entropy functions. Our findings revealed that the hybrid channel can be adeptly tailored to preserve quantum correlations, surpassing the capabilities of its individual components. We also identified optimal parameterizations to attain maximum entanglement from mixed entangled/separable states, even in the presence of local dephasing. Notably, various parameters and quantum features, including non-Markovianity, exhibited distinct behaviors in the context of this hybrid channel. Ultimately, we discuss potential experimental applications of this configuration.

Keywords: thermal reservoir; magnetic field; classical dephasing; static noise; quantum characteristics

Citation: Rahman, A.u.; Yang, M.; Zangi, S.M.; Qiao, C. Probing a Hybrid Channel for the Dynamics of Non-Local Features. *Symmetry* **2023**, *15*, 2189. https://doi.org/10.3390/sym15122189

Academic Editor: Alexey V. Lukoyanov

Received: 1 November 2023
Revised: 2 December 2023
Accepted: 8 December 2023
Published: 12 December 2023

1. Introduction

The transmission of information in quantum information processing is performed using various types of communicating means, which include local and non-local channels [1]. The design of such transmitting channels is important because the resourcefulness of the quantum systems may be lost if the inclusive channels have disorders or no optimal characteristics. In the previous era, various types of channels with various characteristics have been treated separately. However, this would be far from reality, as the characteristics of these various channels can be found at the same place simultaneously, for example the thermal, magnetic, and dephasing effects. In this regard, the thermal interaction picture of the channels has been studied using the concept of Gibb's density matrix operation [2]. Besides this, magnetic fields have also been used to demonstrate the quantum correlations' dynamics explicitly [3]. Most importantly, the local channels have been successfully used for decades for the transmission of information [4]. On the contrary, non-local channels have been investigated, and many efforts for their practical empowerment have been made recently [5]. Compared to the non-local ones, the classical ones have the advantage of being easily implemented, as they do not need any complex design. Pure classical channels, nonetheless, are influenced by certain types of flaws and disorders, such as the impact of surface charge carriers [6], electronic currents [7], and so forth. One of these disorders causes static noise, which will be considered to influence classical channels in the current situation and has been found to completely degrade quantum correlations [8].

We are planning to demonstrate the effectiveness of a complex mixed channel deployed for information transmission; therefore, we will consider simple two-qubit correlations to evaluate our goal. In the emerging discipline of quantum information science, non-classical correlations are now the primary priority of foundational scientific study [9]. A crucial non-local resource known as quantum entanglement explains a particular kind of non-classical correlation among sub-systems of a quantum composite state [10]. When a group of particles interacts spatially such that the quantum states of each particle are mutually exclusive, this is referred to as quantum entanglement. This non-local correlation causes measurements on one part of an entangled pairing and immediately affects the results of measurements on the other. Quantum computers can perform computations that are not conceivable on classical computers because of the advantage that non-local systems can exist in multiple states simultaneously [11]. Researchers are actively developing a quantum Internet and quantum encrypted communications using entanglement [12], which would allow for new varieties of telescopes [13], sensors [14], and ultra-secure broadcasting [15]. Besides, various studies have focused on providing schemes and critical studies on improving the degree of quantum correlations between the sub-systems of the non-local states considering various procedures (for example, see Refs. [16–18]), therefore giving rise to the successful implementation of the quantum protocols. In addition, the information encoded in qubits can be processed more quickly and with less processing power because of the quantum entanglement phenomenon. Recently, it has been demonstrated that quantum coherence and entanglement, two fundamentally dissimilar aspects of quantum theory, are functionally equivalent and have made a variety of quantum technologies possible; therefore, both would remain part of the current study [19].

The uncertainty principle holds that the results of simultaneous measurements of non-commuting observables commonly have an intrinsic lower bound on the uncertainty [20]. This assumption both illustrates how the classical and quantum realms differ and provides the rationale for the ambiguity of quantum mechanics. In essence, it states that you cannot begin preparing a quantum particle whose location and momentum are predictable with certainty, simultaneously [21]. Kennard and Robertson revisited the principle of uncertainty after it had taken the form of a standard deviation and was based on the combined variance of two observables [22]. For example, for two observables $\mathcal{X}$ and $\mathcal{Y}$, the associated uncertainty relation was defined as $\Delta\mathcal{X}\Delta\mathcal{Y} \geq 1/2|\langle[\mathcal{X},\mathcal{Y}]\rangle|$. Furthermore, Deutsch established the well-known version of the entropic uncertainty (EU) relation in 1983 and proposed the uncertainty principle in terms of the Shannon entropy [23]. Afterward, Kraus first proposed another simplified version of the EU relation, which was verified in 1988 by Maassen and Uffink [24,25]. Besides, for different quantum systems and situations, various EU relations have been established. The study of the EU will provide an important aspect of the current hybrid channel to induce uncertainty in the process of quantum information processing [26–28].

The integrability of the Heisenberg Hamiltonian preserves the capacity to identify its precise spectrum [29]. This framework, which Heisenberg first developed, can be considered a recognition of the potential for the advancement of integrable frameworks in low dimensions in both classical and quantum statistical mechanics, as well as field theory [30]. In practice, they have been used in a variety of domains, such as condensed matter physics and high-energy physics [31]. In addition, a large amount of time has been put into studying Heisenberg spin chains recently, and the preservation of quantum correlations has greatly benefited as a result [32]. Quantum information theory methods have been used to study the reduced density matrix of the spin-1 Heisenberg chains, including looking at quantum mutual information [33], quantum discord [34], and the local quantum uncertainty measure [35]. Quantum discord, as opposed to the entanglement of formation, was used to pinpoint the critical regions associated with quantum phase transitions in an XXZ spin chain model [36]. It has been demonstrated that these properties differ from those of thermal entanglement and that thermal quantum correlations can be produced by altering the magnetism and the strength of the Heisenberg interaction coupling strength in

the antiferromagnetic system [37]. However, all these studies have been carried out without considering dephasing. No quantum information configuration considers dephasing; therefore, it is recommended to investigate how much the system is tolerant to dephasing. Indeed, this would allow us to expect the success rate and lifespan of the quantum protocols employed. This made us realize a configuration of the Heisenberg spin-1/2 model, which includes several interactions under local dephasing.

In this work, we considered examining a two-qubit spin state influenced by a thermal and magnetic field [38]. The spin system was further assumed to be characterized by the Dzyaloshinskii–Moriya interaction (DM), Kaplan, Shekhtman, Entin-Wohlman, and Aharony interaction, (KSEA) and the anisotropy parameters' interaction [39,40]. The DM interaction, an antisymmetric exchange interaction that controls chiral spin configurations, is brought on by inversion symmetry breaking in non-centrosymmetric crystal lattice interfaces [41]. On the other hand, the KSEA interaction is caused by the symmetric helical interaction [40]. Besides, the generated quantum correlations need interaction with external channels to be transmitted. As it is known that classical channels are highly destructive for quantum correlations, therefore, we were motivated to investigate the impact of the joint implications of the external thermal–magnetic–classical channel (TMCC) on the quantum correlation dynamics. The reason behind designing such a configuration is to devise a reliable and physically constructional transmitting channel, which we believe will be helpful in quantum correlations' preservation during communication using non-local systems. The entanglement measurement in the spin state is performed by using negativity (NG), which is one of the well-known bipartite entanglement monotones [42]. As stated before, entanglement and coherence are two fundamental correlations of quantum systems. Motivated by this, we also analyzed the dynamics of coherence using the ℓ_1-norm of coherence in the spin system [43]. Quantum systems are always influenced by uncertainty; therefore, we also considered assessing the degree of uncertainty between different observables of the system using EU relations [44]. Besides uncertainty, mixedness disorder is a commonly found phenomenon where most of the quantum correlations in quantum systems are lost because of its emergence. The degree of disorder in the spin state when subjected to the hybrid channel with thermal, magnetic, and local dephasing parts was computed utilizing linear entropy (EN). One of the basic motivations behind the simultaneous measurement of entanglement, coherence, entropic uncertainty, and mixedness disorder is to find the reaction of the assumed hybrid channel towards different non-classical characteristics.

This work is presented as follows: In Section 2, we provide the details of the physical model of the assumed system and channel, along with an introduction to the measurement of two-qubit correlations. Section 3 gives a detailed analysis of the results obtained, and in Section 5, we summarize this work.

2. Physical Model

2.1. Thermal and Magnetic Interaction

We assumed a two spin-1/2 XXZ-type Heisenberg system when exposed to an external homogeneous magnetic field characterized by the DM (D_z) and KSEA (K_z) coupling interactions oriented along the z-axis (as shown in Figure 1). This configuration has the Hamiltonian model given by [32]

$$\mathbf{H} = \Delta_z\left(S_1^z S_2^z\right) + D_z\left(S_1^x S_2^y - S_1^y S_2^x\right) + J\left(S_1^x S_2^x + S_1^y S_2^y\right) + K_z\left(S_1^x S_2^y + S_1^y S_2^x\right) + B\left(S_1^z + S_2^z\right), \quad (1)$$

where S_f^g with $(f = \{1, 2\}, g = \{x, y, z\})$ are the spin-1/2 Pauli matrices of the spin f, Δ_z is the real anisotropy coupling constant describing the symmetric exchange spin–spin interaction in the z-direction, D_z is the DM interaction strength regulating the spin–orbit antisymmetric coupling, and J is the Heisenberg exchange interaction between the spin particles. Note that $J > 0$ ($J < 0$) corresponds to the antiferromagnetic (ferromagnetic) interaction between the spins sites, respectively. Besides, K_z represents the KSEA interaction strength oriented along the $z-$axis responsible for symmetric spin–orbit coupling, while

B is the homogeneous part of the considered magnetic field. The Hamiltonian expression given in Equation (2) in the computational basis $\{|00\rangle, |01\rangle, |10\rangle, |11\rangle\}$ takes the form:

$$\mathbf{H} = \begin{bmatrix} 2B + \Delta_z & 0 & 0 & -2iK_z \\ 0 & -\Delta_z & 2iD_z + 2J & 0 \\ 0 & -2iD_z + 2J & -\Delta_z & 0 \\ 2iK_z & 0 & 0 & -2B + \Delta_z \end{bmatrix}. \tag{2}$$

The corresponding eigenvectors of the Hamiltonian **H** are

$$|\Theta_{1^+,4^-}\rangle = \sqrt{\frac{\Lambda \pm 2B}{2\Lambda}}\left(|00\rangle \pm \frac{2iK_z}{\Lambda \pm 2B}|11\rangle\right), \quad |\Theta_{2^+,3^-}\rangle = \frac{1}{\sqrt{2}}\left(|01\rangle \pm \frac{2J \pm 2iD_z}{v}|10\rangle\right),$$

with $\Lambda = \sqrt{4B^2 + 4K_z^2}$ and $v = \sqrt{4J^2 + 4D_z^2}$. Besides, the eigenvalues of Equation (2) are $E_{1^+,4^-} = \Delta_z \pm \Lambda$, and $E_2 = -\Delta_z + v$.

Using Gibbs's density operator, the thermal state density matrix for the Hamiltonian given in Equation (2) in equilibrium with a thermal reservoir at temperature T using the eigenvectors has the form:

$$\rho(0, T) = \sum_i p_i |\Theta_i\rangle\langle\Theta_i| \tag{3}$$

where $p_i = \frac{e^{-\beta E_i}}{Z}$ is the probability associated with the eigenstate $|\Theta_i\rangle$ with E_i being the eigenenergy corresponding to $|\Theta_i\rangle$ and

$$Z = \mathrm{Tr}\left[\exp\{\frac{-\mathbf{H}}{T}\}\right] = \sum_{i=1}^{4} \exp\left[\frac{-E_i}{T}\right] \tag{4}$$

with Boltzmann's constant $k_B = 1$, ensuring that the probabilities sum up to 1. This representation can be used to see the non-factorable quantum superposition of the thermal Heisenberg state for the two-qubit system in terms of its eigenvalues and eigenvectors. As one can see, the bases in the eigenvectors $|00\rangle$, $|10\rangle$, $|01\rangle$, and $|11\rangle$ are in superposition of each other, hence suggesting that the considered two spins are in the entanglement domain.

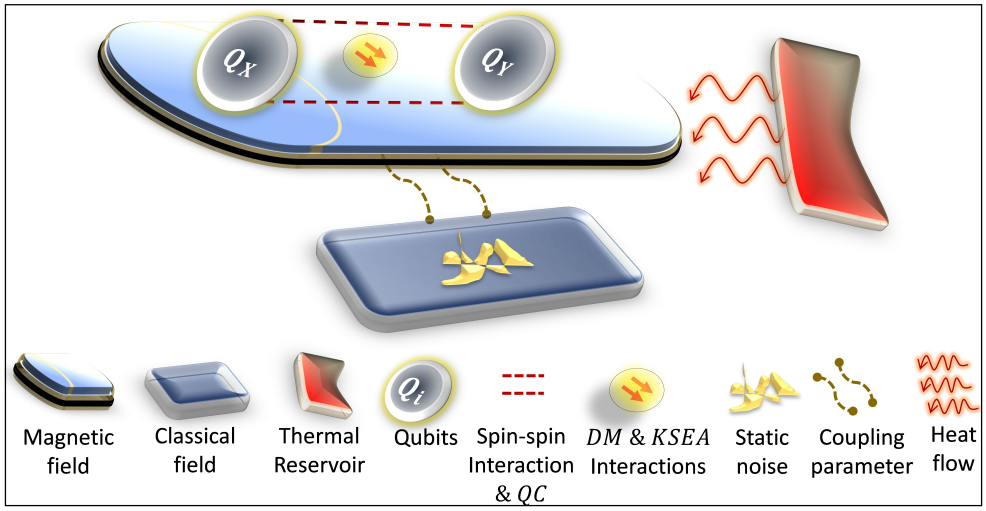

Figure 1. The physical model of the hybrid channel with thermal, magnetic, and classical dephasing parts controlled by static noise employed for the dynamics of the two-qubit Heisenberg spin state characterized by various parameters, such as spin–spin, DM, and KSEA interaction.

Finally, the thermal density matrix $\rho(0,T)$ in the computational basis has the form:

$$\rho(0,T) = \begin{bmatrix} \rho_{11} & 0 & 0 & \rho_{14} \\ 0 & \rho_{22} & \rho_{23} & 0 \\ 0 & \rho_{23}^{*} & \rho_{33} & 0 \\ \rho_{41}^{*} & 0 & 0 & \rho_{44} \end{bmatrix}. \tag{5}$$

The corresponding entries are given by

$$\begin{aligned}
\rho_{11} &= \frac{1}{Z} e^{-\frac{\Delta_z}{T}} \left(\cosh(\varphi) - \frac{B \sinh(\varphi)}{\sqrt{B^2 + K_z^2}} \right), \\
\rho_{14} = \rho_{41}^{*} &= \frac{1}{Z\sqrt{B^2 + K_z^2}} i K_z e^{-\frac{\Delta_z}{T}} \sinh(\varphi), \\
\rho_{22} = \rho_{33} &= \frac{1}{Z} e^{\Delta_z / T} \cosh(\varpi), \\
\rho_{23} = \rho_{32}^{*} &= \frac{1}{Z\sqrt{D_z^2 + J^2}} (-J - i D_z) e^{\Delta_z / T} \sinh(\varpi), \\
\rho_{44} &= \frac{1}{Z} e^{-\frac{\Delta_z}{T}} \left(\frac{B \sinh(\varphi)}{\sqrt{B^2 + K_z^2}} + \cosh(\varphi) \right),
\end{aligned} \tag{6}$$

where $\varphi = \frac{1}{T}(2\sqrt{B^2 + K_z^2})$, $\varpi = \frac{1}{T}(2\sqrt{\mathrm{Dz}^2 + J^2})$ and partition function $Z = 2e^{-\frac{\Delta_z}{T}}(e^{\frac{2\Delta_z}{T}} \cosh(\varpi) + \cosh(\varphi))$.

2.2. The Exposure to a Classical Channel

Here, we provide the exposure of the two-qubit spin state to a common classical environment driven by static noise. In the present case, the Hamiltonian, which governs the current physical model, is written as [45]

$$\mathbf{H}_{XY} = \mathbf{H}_X \otimes \mathrm{I}_Y + \mathrm{I}_X \otimes \mathbf{H}_Y, \text{ with } \mathbf{H}_{\mathcal{P}} = \begin{bmatrix} \Delta_{\mathcal{P}}\lambda + \epsilon & 0 \\ 0 & \epsilon - \Delta_{\mathcal{P}}\lambda \end{bmatrix}, \tag{7}$$

where $\mathbf{H}_{\mathcal{P}}$ $(\mathcal{P} = X, Y)$ denotes the Hamiltonian state of the sub-system $\mathcal{P}$, ϵ is the equal energy splitting between the sub-systems, I is the 2×2 identity matrix, λ is the coupling constant, $\Delta_{\mathcal{P}}$ regulates the stochastic behavior of the classical field and is flipping between ± 1, and S^z is the spin-Pauli matrix.

For the time evolution of the system, we used the following time-unitary operator, where

$$U_{XY}(t) = \exp\left\{ -i \int_{t_0}^{t} H(z) dz \right\} = \begin{bmatrix} U_{11} & U_{12} & U_{13} & U_{14} \\ U_{12} & U_{11} & U_{14} & U_{13} \\ U_{13} & U_{14} & U_{11} & U_{12} \\ U_{14} & U_{13} & U_{12} & U_{11} \end{bmatrix}, \tag{8}$$

which is the time-unitary matrix with $\hbar = 1$, and the matrix entries are

$$\begin{aligned}
U_{11} &= \exp\{-2it\epsilon\} \cos(\Delta_X \lambda t) \cos(\Delta_Y \lambda t), \\
U_{12} &= -i \exp\{-2it\epsilon\} \cos(\Delta_X \lambda t) \sin(\Delta_Y \lambda t), \\
U_{13} &= -i \exp\{-2it\epsilon\} \sin(\Delta_X \lambda t) \cos(\Delta_Y \lambda t), \\
U_{14} &= -\exp\{-2it\epsilon\} \sin(\Delta_X \lambda t) \sin(\Delta_Y \lambda t).
\end{aligned} \tag{9}$$

To obtain the time-evolved state of the system for the initial thermal state density matrix $\rho(0,T)$ given in Equation (6) when exposed to an identical channel, i.e., $\Delta_X = \Delta_Y$, we use [45]

$$\rho_{X,Y}(t,T) = U_{XY}(t)\rho(0,T)U_{XY}(t)^\dagger \rightarrow \rho(t,T) = U_{XX}(t)\rho(0,T)U_{XX}(t)^\dagger, \tag{10}$$

and explicitly, the above equation takes the following shape:

$$\rho(t,T) = \begin{bmatrix} \rho_{11} & 0 & 0 & e^{-4i\Delta_X\lambda t}\rho_{14} \\ 0 & \rho_{22} & \rho_{23} & 0 \\ 0 & \rho_{32}^* & \rho_{33} & 0 \\ \rho_{41}^* e^{4i\Delta_X\lambda t} & 0 & 0 & \rho_{44} \end{bmatrix}. \tag{11}$$

The Influence of Classical Static Noise Disorder

Next, we provide the application and influence of the static noise on the time-evolved state of the spin system. In this regard, static noise is primarily characterized by Δ_Q, namely the disorder parameter. This noise has the probability distribution function $\mathcal{O}(\delta) = 1/\Delta_Q$ and exhibits the range $|\delta - \delta_o| \leq \Delta_Q/2$, where δ_o denotes the mean value of the probability distribution function [46]. The autocorrelation function of the stochastic parameter $\langle \delta\Delta(t)\Delta(0)\rangle = \Delta_Q^2/2$ reveals crucial insights into the nature of the stochastic process. This expression implies that the fluctuations in $\Delta(t)$ exhibit persistence over time, as the autocorrelation function does not decay to zero, but instead, maintains a value of $\Delta_Q^2/2$. This characteristic behavior gives rise to a power spectrum dominated by a δ function sharply peaking at zero frequency. The presence of this distinct peak signifies a longer characteristic timescale associated with the noise, surpassing the timescales of the system–environment coupling. Consequently, the static noise displays non-Markovian characteristics, suggesting that the temporal correlations within the stochastic parameter persist over timescales comparable to or longer than the timescales of the underlying system–environment interactions. This nuanced understanding of the noise properties provides valuable insights into the intricacies of the dynamical processes and sheds light on the non-Markovian nature of the associated stochastic fluctuations. However, it should be noted that, for the practical deployment of the configuration, besides noise, other resources related to the design should be taken into account. For example, in a study, the non-Markovian behavior of the Rabi pulses was found to be deeply dependent on the configuration, including the dot dimensions and the waveform shapes of the applied laser [47]. Besides a particular type of dephasing, the connection between cavity decay and the phonon-induced renormalization of the light–matter interaction has also been found to affect the transitions of the state [48].

To evaluate the impact of the static noise on the dynamics of the spin state, the time-evolved state density matrix was averaged over all possible noise configurations. Therefore, we integrated the matrix in Equation (11) between $r^+ = \delta_o - \Delta_Q/2$ and $r^- = \delta_o + \Delta_Q/2$ as [8]

$$\rho_{st}(t,T) = \int_{r^-}^{r^+} \frac{1}{\Delta_Q}\rho(t,T)d\Delta_X = \begin{bmatrix} \rho_{11} & 0 & 0 & \hat{\rho}_{14} \\ 0 & \rho_{22} & \rho_{23} & 0 \\ 0 & \rho_{23}^* & \rho_{33} & 0 \\ \hat{\rho}_{41}^* & 0 & 0 & \rho_{44} \end{bmatrix}, \tag{12}$$

where $\rho_{ii}(ii = 11, 22, 33, 44, 23)$ remains the same as given in Equation (6). However, $\hat{\rho}_{14} = \hat{\rho}_{41}^* = \frac{\rho_{14}e^{-4i\delta_o\lambda t}\sin(2\Delta_Q\lambda t)}{2\Delta_Q\lambda t}$.

Note that the final matrix given in Equation (12) represents the two-spin system simultaneously influenced by a thermal, magnetic, and classical channel. Note that the off-diagonal matrix elements are included now with dephasing terms; hence, the coherence loss of the systems is included. Therefore, the loss of entanglement, the rise of the uncertainty,

and the mixedness in the state with time would give us a realistic model in comparison, if one only considered the case of magnetic and thermal interaction.

2.3. Quantum Criteria Quantifiers

2.3.1. Bipartite Negativity

Multiple quantitative factors have been developed that demonstrate the level of entanglement in a quantum state. For example, negativity (NG) has been investigated as a valuable and calculable witness to entanglement for any pure and mixed states. The Peres–Horodecki separability criterion serves as the foundation for this. On a rescaled scale, NG for a statistical ensemble ρ_{XY} is defined as [49]

$$\mathrm{NG} = 2\sum_i |\mathcal{Q}_i|, \tag{13}$$

where $\mathcal{Q}_i$ are the negative eigenvalues of the partially transposed density matrix $\rho_{XY}^{T_X}$ with respect to sub-system X. The state is maximally correlated if $NG = 1$, while for $NG = 0$, the state will become separable [45].

2.3.2. The Entropic Uncertainty Measure

Consider Bob and Alice to be the two users. Alice receives a qubit in the desired quantum state created by Bob. Alice must now select one of the two measurements and notify Bob of her selection. We can now lower the result's uncertainty by using Bob's measurement data [22]. The uncertainty standard deviation for two observables $\mathcal{X}$ and $\mathcal{Y}$ can be represented as: $\Delta\mathcal{X}\Delta\mathcal{Y} \geq \frac{1}{2}|\langle[\mathcal{X},\ \mathcal{Y}]\rangle|$ [23,26–28].

Instead of utilizing the standard deviation to describe uncertainty, Deutsch suggested the entropic uncertainty relation for every pair of observables, as shown in the above equation. Based on Deutsch's method, Maassen and Uffink created a tighter entropic uncertainty formulation, which can be represented as $S(\mathcal{X}) + S(\mathcal{Y}) \geq \log_2 c(\mathcal{X};\mathcal{Y})$ [25], where $S(K)(K = \mathcal{X}, \mathcal{Y})$ is known as the Shannon entropy denoting the probability distribution of measuring the observable K, while $c(\mathcal{X};\mathcal{Y}) = \max_{a,\ b} |\langle\psi|\phi\rangle|^2$ is the maximal overlap between the eigenvectors ψ and ϕ of the two non-degenerate observables.

A new definition presented by Renes et al. and Berta et al. considered the entropic uncertainty relations in composite systems and proposed a quantum-memory-assisted entropic uncertainty relation [50,51]. Therefore, the quantum-memory-assisted entropic uncertainty regarding system A is reproduced corresponding to q quantum memory B with a tighter bound and has the form

$$S(\mathcal{X}|B) + S(\mathcal{Y}|B) \geq S(A|B) - \log_2 c(\mathcal{X};\mathcal{Y})), \tag{14}$$

where $S(\mathcal{X}|B) = S(\rho_{\mathcal{X}B}) - S(\rho_B)$ is the conditional von Neumann entropy of the system after the unilateral measurement is applied on $\mathcal{X}$ on sub-system A. Note that the same procedure can be carried out for $\mathcal{Y}$ as well. The associated post-measurement state now can be written as

$$\rho_{\mathcal{X}B} = \sum_i (|\psi\rangle\langle\psi| \otimes I)\rho_{AB}(|\psi\rangle\langle\psi| \otimes I). \tag{15}$$

The conditional entropy $S(A|B)$ computes the correlation between sub-system B owned by its memory system A.

Equation (14) comprises the entropic uncertainty (EU) on the left-hand side and entropic uncertainty lower bound on the right-hand side. In the current case, we only emphasize measuring the left-hand side of the uncertainty relations.

2.3.3. ℓ_1-Norm of Coherence

Different metrics, including the distance metric [52], the relative entropy of coherence [32], and purity can be used to evaluate the coherence. The ℓ_1-norm is a reliable

coherence monotone and a coherence criterion [32]. Besides, the ℓ_1-norm coherence for a two-qubit state $\rho = \sum_{X,Y} \rho_{XY}|X\rangle\langle Y|$ is the sum of all the off-diagonal entries as [43]

$$LC(t) = \sum_{X \neq Y} |\rho_{XY}|, \tag{16}$$

where $|\rho_{XY}|$ is the absolute value of the elements of the density matrix ρ_{XY}.

2.3.4. Linear Entropy

Linear entropy, a simple-to-evaluate scalar field, is used to measure the mixedness of quantum states. For example, by approximating the $\log_2 \rho_{XY}$ of $S(\rho_{XY})$ with the first-order term, i.e., $\rho_{XY} - 1$ in the Mercator series, one may obtain

$$EN(t) = -\operatorname{Tr}[\rho_{XY} \log_2 \rho_{XY}]. \tag{17}$$

For the next-to-last equality, the density matrix's unit trace feature ($\operatorname{Tr}[\rho_{XY}] = 1$) is used.

3. Results

This section is devoted to exploring the numerical results obtained for the dynamics of the two-qubit spin state influenced by an external TMCC configuration. Additionally, the impact of various parameters such as the anisotropy, spin coupling strength, DM and KSEA interactions, as well as external noise parameters of the static noise was studied. Utilizing the NG, EU, LC, and EN functions given in Equations (13), (14), (16), and (17), we explored the dynamics of entanglement, quantum memory, coherence, and entropy in the spin system. All the functions were evaluated for the final density matrix obtained in Equation (12).

In Figure 2, we analyze the dynamics of entanglement, entropic uncertainty, coherence, and entropy in a two-spin state when coupled with an external TMCC. Initially, the state remains maximally entangled and coherent, as $NG = LC = 1$. The depicted entropic uncertainty and entropy in the state remain zero initially, as $EU = EN = 0$. After the onset, the action of the joint TMCC appears, and as a result, entanglement, as well as coherence become easily lost. In agreement, the EU and EN remained increasing functions of the entropic uncertainty and disorder in the system. The overall dynamical maps of the spin state correlations remained non-Markovian; however, the degree of non-Markovianity shown by each measure differed. For example, the NG and LC functions showed a large number of entanglement and coherence revivals. This suggested that the two-qubit system and coupled fields strongly support information exchange between them. On the other hand, the non-Markovian behavior shown by the EU and EN functions remained weaker. Therefore, the NG and LC functions were more sensitive than the EU and EN functions and recorded the least exchange of attributes between the state and the field. Besides, the NG and LC functions showed anti-correlation with the EU and EN functions, as both pairs evolved in opposite directions to each other. Furthermore, for the increasing values of the disorder parameter Δ_Q, the entanglement and coherence remained fragile and became easily lost in the state. On the other hand, the uncertainty between the observables of the particles and associated mixedness disorder in the state was enhanced by the increasing strength of Δ_Q. However, it was noticeable that the rate of revivals was directly dependent on Δ_Q. The phenomenon of the sudden death and birth of entanglement occurred repeatedly. Finally, the entanglement and coherence functions seemed to completely decay with time, while the uncertainty and entropy functions achieved a final higher saturation level. One of the studies that comprehensively investigated superconductivity showed that this phenomenon was enhanced by increasing the degree of the disorder correlations [53]. As we only focused on the impact of static noise here, therefore, we comprehended that any physical deployment of the configuration with static noise would also need to consider

other related impacts besides the disordered parameter studied here. Note that the static noise disorder decaying quantum coherence can also be from the study given in Ref. [54].

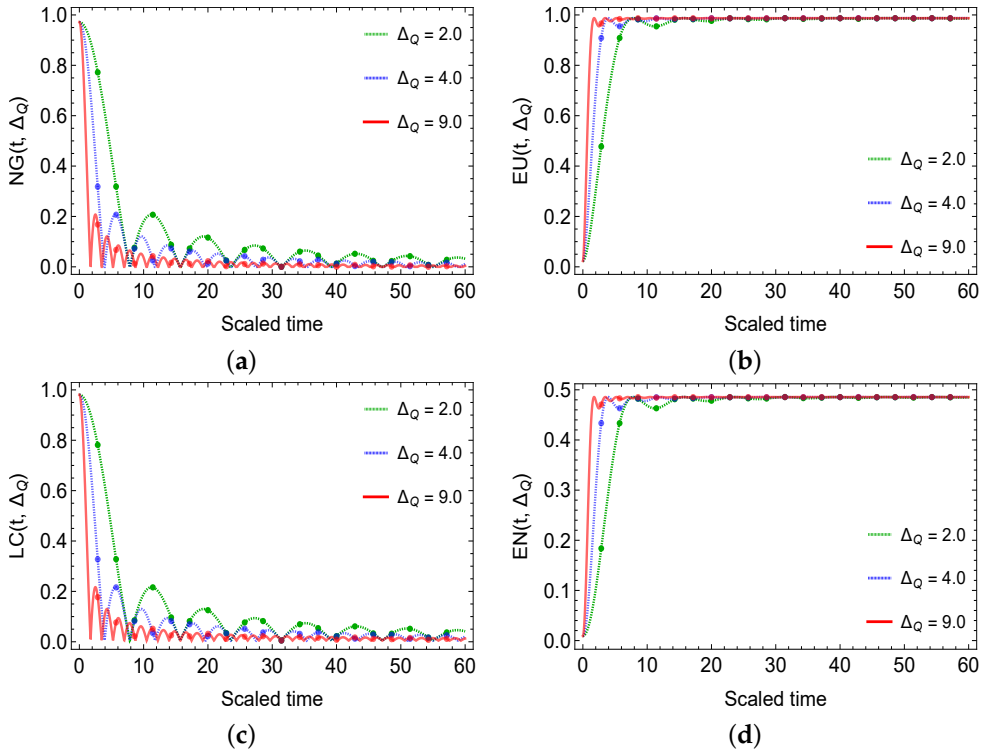

Figure 2. Dynamics of negativity (**a**), entropic uncertainty (**b**), ℓ_1-norm coherence (**c**), and linear entropy (**d**) as functions of static noise disorder parameter Δ_Q against time in a two-spin system influenced by an external TMCC. For all the plots, we set $\lambda = 0.1$, $K_z = 5$, and $J/T/D_z/J_z/\Delta_z/B/J/ = 1$.

In Figure 3, the impact of weak, as well as strong coupling strength λ of the classical channel on the dynamics of entanglement, coherence, entropic uncertainty, and entropy disorder in a two-spin system when exposed to an external magnetic field is studied. Initially, the two-qubit spin system remains maximally entangled and coherent as the functions are $NG = LC = 1$. On the contrary, $EU = EN = 0$ suggests that the system is free of entropic uncertainty and mixedness. As the interaction between the external TMCC and the two-qubit spin system starts, the initial maximal correlations in the state decrease. The speed of decay of entanglement and coherence is regulated by the coupling strength of the classical field. The strong coupling of the spin state with the classical environment resulted in a quicker decay of correlations and vice versa. Besides, the non-Markovian behavior of the classical fields is highly enhanced in the strong coupling regimes, while becoming negligible at the weaker coupling strength end. Likewise, the uncertainty and entropy disorder increased with higher speeds as λ increased. Finally, the speed of entropic uncertainty and entropy is directly related to the decay rate of the entanglement and coherence, therefore showing an anti-correlation between the two pairs of phenomena. The phenomenon of the sudden death and birth of entanglement varied with the varying strengths of coupling strength regimes of the classical field. Compared to Figure 2, the decay observed in the current case had the least values. Hence, quantum correlation decay can be highly controlled by tuning the coupling intensity between the classical field and the two-qubit state. However, the fact remains consistent that both the parameters, namely the disorder Δ_Q and coupling parameter λ, regulated the rate of the sudden death and birth of the entanglement and coherence. Finally, for the higher λ values, the entanglement and coherence became completely lost, hence suggesting maximum entropy disorder and absolute separability in the state. From the current study, we noticed that the coupling

strength of the channel induced a certain degree of decay in the quantum features, which was also confirmed for quantum coherence in the study [54].

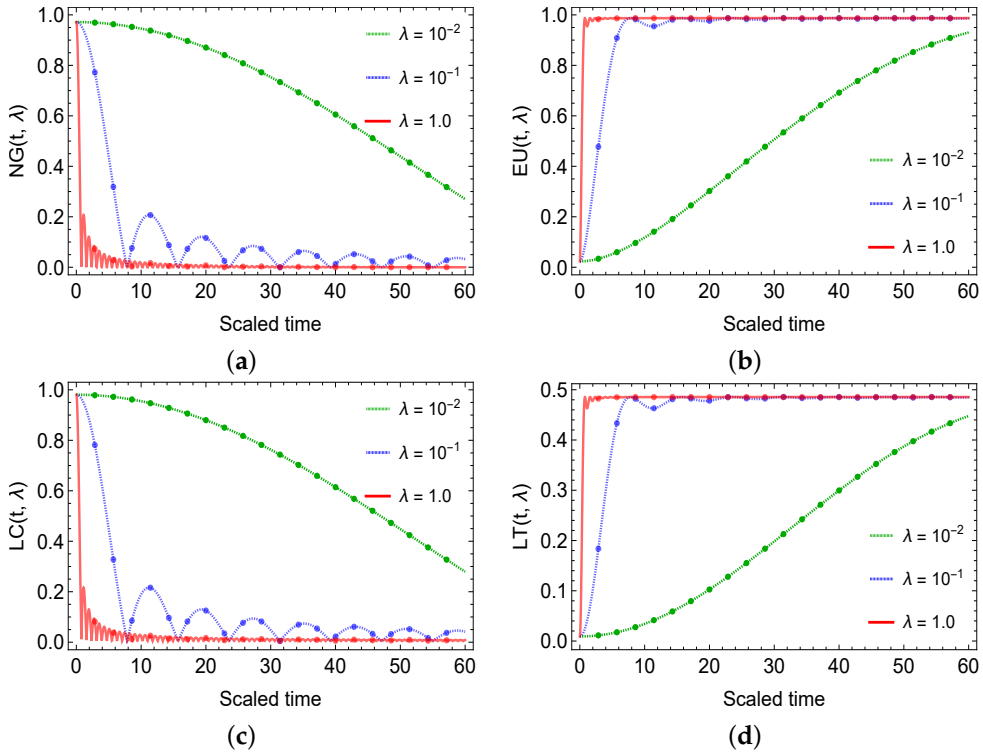

Figure 3. Dynamics of negativity (**a**), entropic uncertainty (**b**), ℓ_1-norm coherence (**c**), and linear entropy (**d**) as functions of classical field's coupling strength λ against time in a two-spin state influenced by an external TMCC. For all the plots, we set $\Delta_Q = 2$, $K_z = 5$, and $J/T/D_z/J_z/\Delta_z/B/J = 1$.

The temperature influence on the dynamics of entanglement, coherence, entropic uncertainty, and entropy is analyzed in a system of a two-qubit spin state when subjected jointly to TMCC in Figure 4. The influence was taken into account when the temperature of coupled fields was assumed at different fixed higher and lower values. The difference between the dynamics of the entanglement, coherence, uncertainty, and disorder functions was significant. As seen for the higher temperature values $(T = 7)$, the initial entanglement and coherence values decreased while the original entropic uncertainty and mixedness in the state increased, hence contradicting the characteristic properties of disorder parameter Δ_Q (Figure 2) and λ (Figure 3), which do not influence the initial values of the inclusive functions. Besides this, the dynamical maps of entanglement comprise repeated sudden death and birth revivals for the lower temperature values $(T = 0.1)$. On the contrary, the entanglement decayed exponentially with time for the higher temperature values. The coherence function LC deviated from the entanglement NG function and showed revivals of coherence, even at the higher temperature values, hence suggesting the strengthened nature of coherence in the spin state compared to the associated entanglement. Unlike the cases in Figures 2 and 3, entanglement and coherence remained preserved for longer intervals of time in the current case, especially for the higher temperature values. The impact of increased temperature has been found to induce quantum discord in a dimerized spin chain, therefore agreeing with the current results that, even at high temperatures, quantum correlations can be kept preserved [55]. It is interesting to note that, for the higher temperature values, the initial values of the entanglement and coherence functions decreased, but remained largely preserved for the latter interval of time. Likewise, the entropic uncertainty and entropy functions were initially directly affected by the temperature; however, for the higher temperature values, the uncertainty and mixedness in the state reduced at the latter intervalof time. However, for the lower entropic uncertainty and

mixedness, one must keep the temperature at minimum values. In comparison, the NG function's revival character seemed very susceptible to the increasing values of temperature and became easily dissipated.

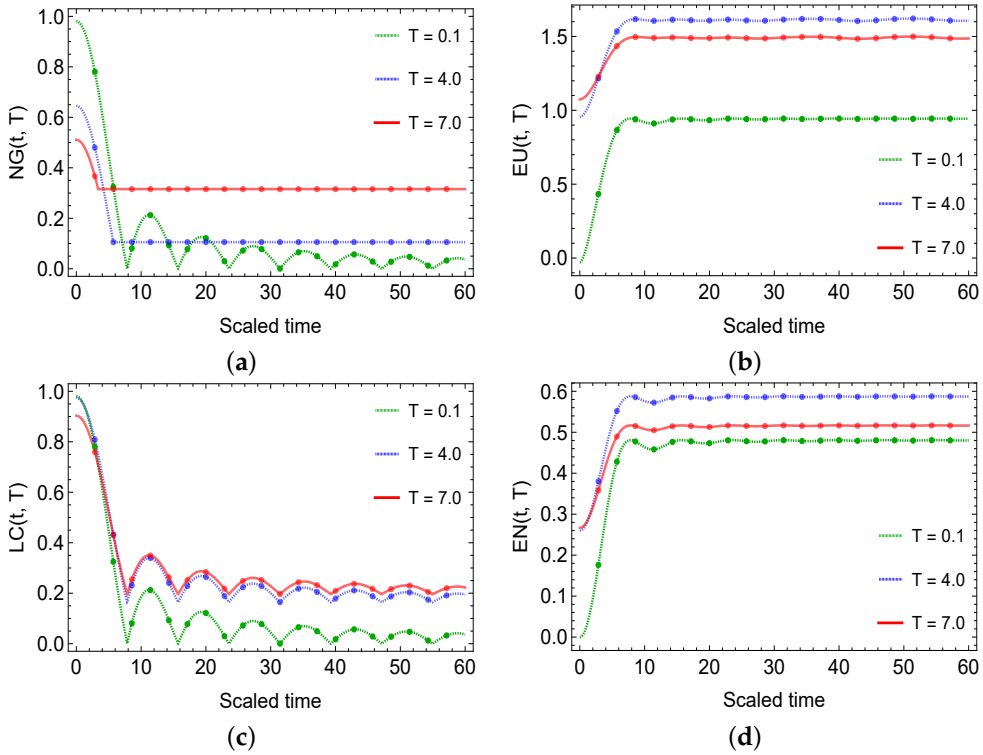

Figure 4. Dynamics of negativity (**a**), entropic uncertainty (**b**), ℓ_1-norm coherence (**c**), and linear entropy (**d**) as functions of temperature T against time in a two-spin system influenced by an external TMCC. For all the plots, we set $\Delta_Q = 2$, $\lambda = 0.1$, $K_z = 5$, and $J/D_z/J_z/\Delta_z/B/J = 1$.

Figure 5 discloses the dynamics of entanglement, coherence, entropic uncertainty, and mixedness in a two-qubit spin system coupled with TMCC. In particular, the impact of the KSEA interaction (K_z) fixed to different strengths was evaluated on the dynamics of the system. The dynamical maps of the NG, EU, LC, and EN functions seem increasingly different from those observed in Figures 2–4. As can be seen, a higher degree of entanglement and coherence preservation limit was achieved for a lower KSEA interaction strength $K_z = 1.0$. In close connection, a lower limit of entropic uncertainty and mixedness in the two-qubit state was observed at $K_z = 1.0$. However, for the increasing strength of the KSEA interaction ($K_z = 5$), the entanglement, as well as the coherence function suffered a greater decay. This contradicts most of the previous findings obtained in Refs. [32,56,57], where, for the increasing strength of K_z, quantum correlations in the state became more preserved. One of the reasons behind this can be the changes brought up by the KSEA interaction in the spin structures, as evidenced in Ref. [58], where cycloidal spin structures were distorted by this interaction. However, it was noticeable that the increasing KSEA interaction strength improved the revival character of the NG, EU, LC, and EN functions. In particular, for $K_z = 5.0$, the entanglement and coherence functions started facing sudden deaths and births with decreasing amplitudes. Besides, entanglement for $K_z = 3.0$ dissipated completely and only agreed with the entropy disorder in the state. The coherence function, on the other hand, remained non-zero for $K_z = 3.0$ and agreed with the entropic uncertainty function. As can be seen for $K_z = 3.0$, the EU function showed minimal uncertainty between the observables of the state compared to that seen at $K_z = 5.0$. Hence, the KSEA interaction of the external magnetic field most likely differently affects different quantum criteria. The revivals in the entanglement and coherence functions suggest strong information exchange between the two-qubit spin state and coupled fields. Therefore,

with the increasing KSEA interaction, one can reverse the information lost from the system, and the conversion of free classical states into resourceful non-local states is feasible. Finally, entanglement and coherence seemed indefinitely preserved in the two-qubit state for the lower K_z values, which may greatly benefit the quantum-information-processing protocols. Besides, the decay rates of entanglement and coherence were found to be proportional to the increasing speed of entropic uncertainty and mixedness in the state, therefore showing an inverse relation between them. In comparison, the *LC* followed by the *NG* function caught a greater number of revivals compared to the *EU* and *EN* functions. This means that the *NG* and *LC* are highly sensitive to the stimuli caused by the external TMCC.

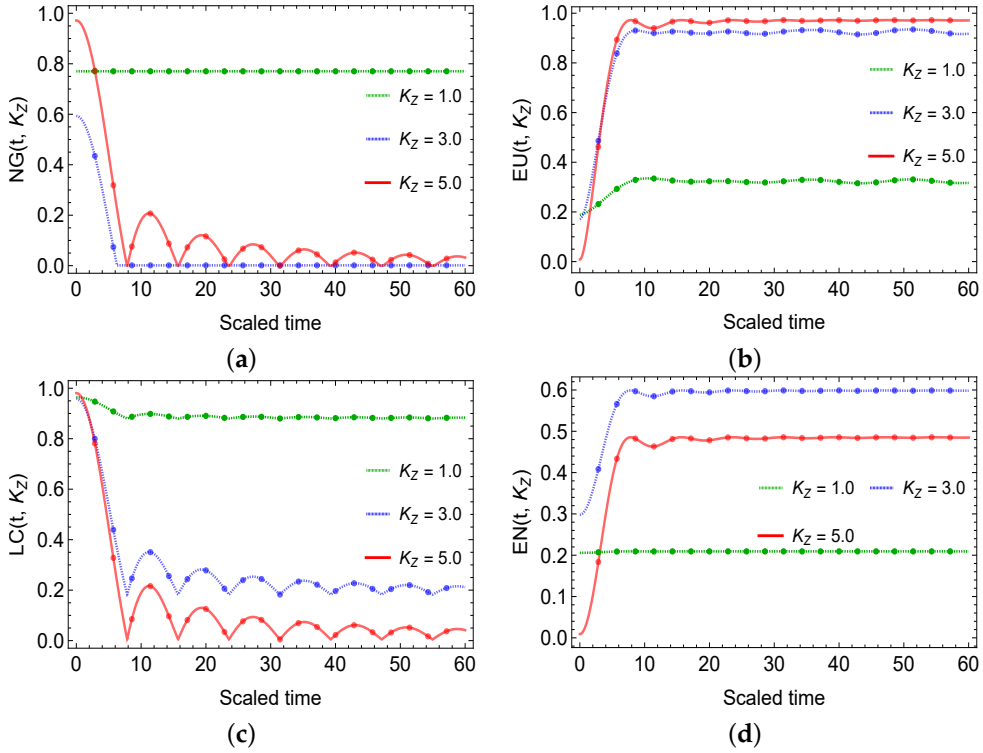

Figure 5. Dynamics of negativity (**a**), entropic uncertainty (**b**), ℓ_1-norm coherence (**c**), and linear entropy (**d**) as functions of KSEA interaction along the *z*-axis K_z against time in a two-spin state influenced by an external TMCC. For all the plots, we set $\Delta_Q = 2$, $\lambda = 0.1$, and $J/D_z/J_z/\Delta_z/B/J = 1$.

In Figure 6, we probe the influence of different fixed values of magnetic field strength parameter B on the time evolution of the two-spin system when connected with TMCC. At the onset, the state preserved different values of initial entanglement and coherence. For the higher magnetic field strengths, $B = 9.0$, the initially encoded entanglement and coherence decreased, while the entropic uncertainty and mixedness in the state increased. Therefore, the external magnetic field negatively affected the preservation of quantum correlations in the spin state. Besides the initial level, the time evolution of the entanglement and coherence functions was also negatively affected by the magnetic field. As seen for the higher magnetic field strength, $B = 9.0$, entanglement and coherence revived at a lower level, while the entropic uncertainty and mixedness functions reached a higher saturation level. On the contrary, for the lower magnetic field strength, $B = 1.0$, the entanglement and coherence functions seemed more preserved, and the reverse can be seen for the entropic uncertainty mixedness in the state. In a similar study, the authors confirmed that the proper tuning of the magnetic field can lead to non-zero discord [59], as we found also in our current study for entanglement and coherence. The revival rate, on the other hand, was not disturbed by the different strengths of the external magnetic field and remained the same. However, for the lower B values, the revivals in entanglement and coherence had a higher amplitude, therefore predicting the larger information flow between the two qubits

and coupled fields. In comparison, the impact of magnetic field parameter B matched that of the disorder parameter Δ_Q and coupling constant λ (especially the higher λ values) of the classical field, as illustrated in Figures 2 and 3, respectively. As can be seen in the mentioned cases, the entanglement functions quickly decayed, while the emergence of uncertainty disorder in the state occurred faster. Therefore, for the optimal longer and greater degree of quantum correlations in the two-qubit state, one must tune the external magnetic field to the least values. Moreover, in agreement with Figures 2–5, we found an anti-correlation between the growing EU and EN functions with the decaying NG and LC functions. Finally, the decreasing amplitudes of the revivals in entanglement and coherence showed that the state at the final intervalsof time will become fully separable with a higher degree of uncertainty and disorder, depending on the strength of the external magnetic field.

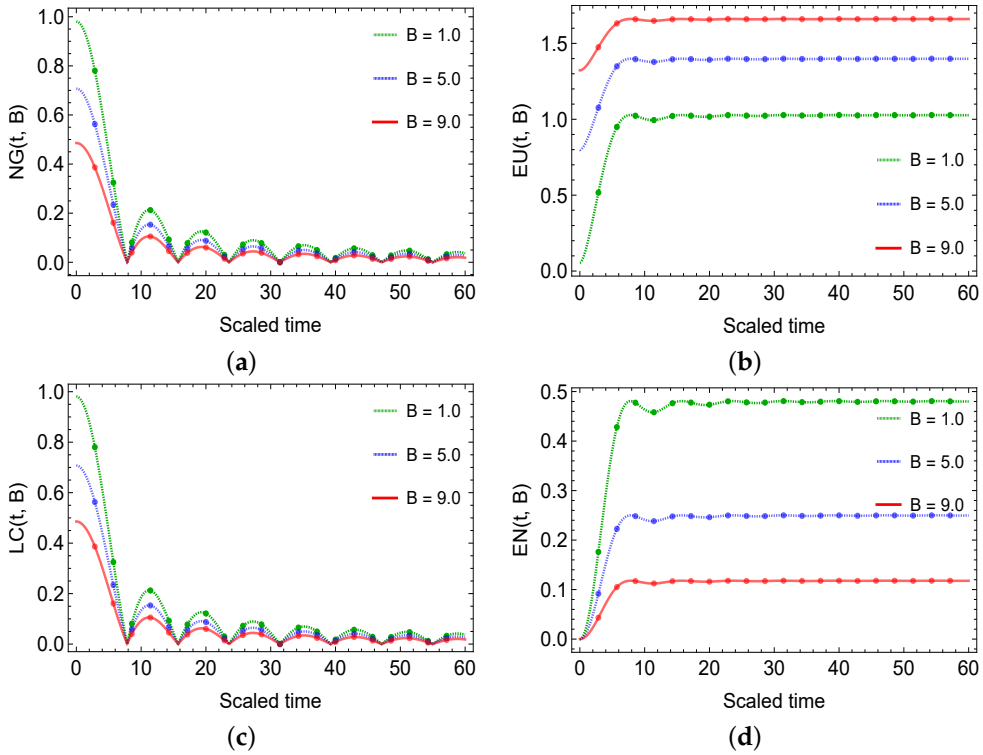

Figure 6. Dynamics of negativity (**a**), entropic uncertainty (**b**), ℓ_1-norm coherence (**c**), and linear entropy (**d**) as functions of magnetic field strength B against time in a two-spin state influenced by an external TMCC. For all the plots, we set $\Delta_Q = 2$, $\lambda = 0.1$, $K_z = 5$, and $J/D_z/J_z/\Delta_z/J = 1$.

When coupled with the TMCC configuration, the impact of different fixed values of the DM interaction strength D_z on the dynamics of entanglement, coherence, entropic uncertainty, and entropy functions in a two-qubit spin state is investigated in Figure 7. The role of the D_z parameter in the dynamics of entanglement, coherence, uncertainty, and mixedness was found to be contradicting all the cases studied in Figures 2–6. In all the previous figures, the parameters associated with the classical, as well as the magnetic field seemed to negatively affect the initially encoded quantum correlations and positively accelerate the uncertainty and mixedness function. However, the opposite occurred in the current case, where, for the increasing strength of D_z, the entanglement and coherence functions were enhanced, while the uncertainty and entropy functions were suppressed. Precisely, the two-qubit state for the initial, as well as for the later interval of time remained maximally entangled and coherent for $D_z = 6.0$. In agreement, for $D_z = 6.0$, the state remained indefinitely free of the uncertainty and mixedness disorder, which is interesting. However, for $D_z < 5$, the agreement between the entanglement and coherence functions vanished, where the prior one became non-maximal, while the latter one remained maximal.

It is also interesting that, for $D_z = 3.5$, entanglement showed a quick drop and seemed completely dissipating while the coherence remained preserved with a non-zero value. The initial, as well as the later dynamical map of entanglement functions seemed in close connection with the entropy function. On the other hand, the *LC* function and the associated dynamical outlooks seemed similar to that obtained for the uncertainty in the state. As seen for different values of D_z, the initial level of entanglement and entropy differed. However, for a similar situation, the initial levels of coherence and uncertainty corresponded to each other, and both functions started from maximal coherence and zero uncertainty points, respectively. The revival characteristic of the entanglement and coherence appeared enhanced for the lower D_z values and, so, the opposite. Finally, by regulating D_z to higher values, the state may be kept maximally entangled and coherent while free from uncertainty and entropy disorder, while detuning of D_z may cause the initial, as well as the latter preserved levels of quantum correlations to decrease, while enhancement in the uncertainty and entropy in the state may occur. Besides this, the fact remains consistent that there is an anti-correlation between the entanglement and coherence pair with the uncertainty and entropy pair. The results in Ref. [60] can be viewed as a verification of the current finding, where the authors found enhancement of the entanglement by increasing the DM interaction to a suitable strength.

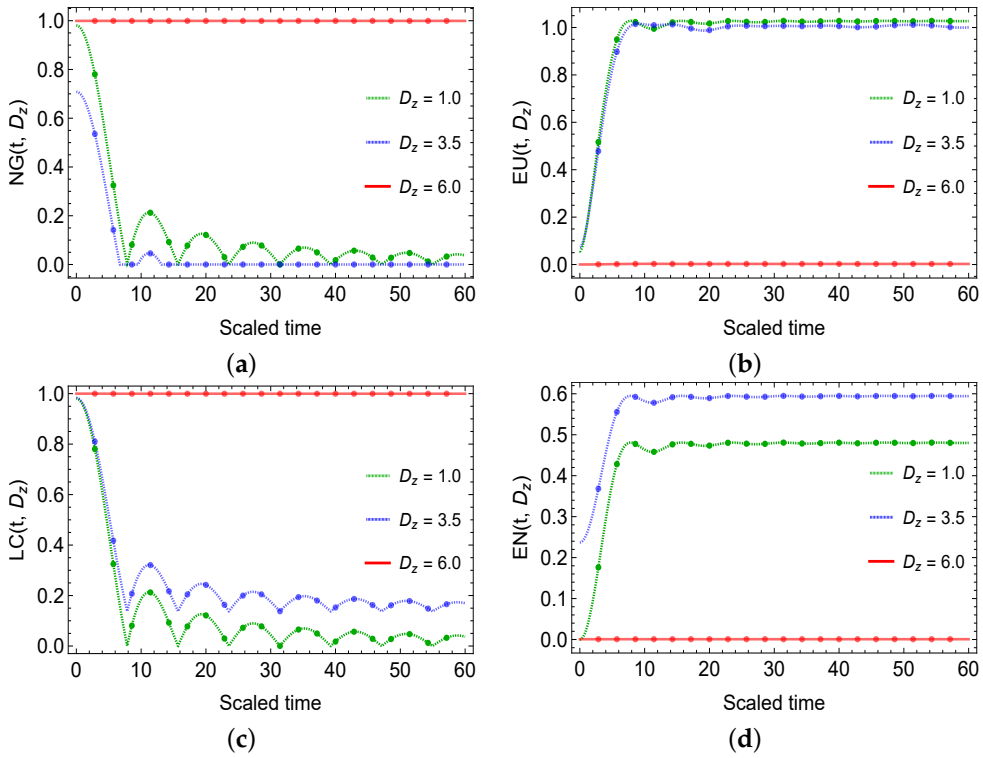

Figure 7. Dynamics of negativity (**a**), entropic uncertainty (**b**), ℓ_1-norm coherence (**c**), and linear entropy (**d**) as functions of DM interaction strength along the z-axis D_z against time in a two-spin state influenced by an external TMCC. For all the plots, we set $\Delta_Q = 2$, $\lambda = 0.1$, $K_z = 5$, and $J/D_z/\Delta_z/B/J = 1$.

In Figure 8, we address the dynamics of entanglement, coherence, entropic uncertainty, and entropy mixedness in a two-spin system when exposed to an external TMCC. The influence of different fixed values of the anisotropy factor of the two-spin system on the dynamics of the two-qubit correlations was obtained in detail. The dynamical outlook obtained for different values of Δ_z seemed in agreement with that obtained in Figure 7 for different fixed values of the DM-interaction. However, the results obtained contradicted the results obtained in Figures 2–6, where strong entanglement and coherence decay are detected. For the increasing anisotropy strengths, entanglement and coherence remained

highly preserved. For instance, see the slopes of entanglement and coherence at $\Delta_z = 6.0$, where the state remains maximally entangled and coherent indefinitely. In close connection, for $\Delta_z = 6.0$, the *EU* and *EN* functions remained zero, hence predicting zero-entropic uncertainty and disorder in the spin state. It is interesting to note that, for $\Delta_z = 3.5$, coherence improved, while entanglement was witnessed to decay completely in a short time, and the same is also witnessed in Figure 7 against D_z. The improvement in entanglement with the increase in Δ_z was also observed in Ref. [60], however without reaching the maximal degree of quantum correlation. Entanglement and coherence showed repeated sudden death and birth revivals at $\Delta_z = 1.0$, therefore predicting strong information exchange between the two-qubit state and coupled fields. The entropy function *EN* agreed with the entanglement function *NG* (where entanglement completely decayed) and showed that, for $\Delta_z = 3.5$, the entropy in the system became maximum. On the other hand, the *LC* and *EU* functions agreed and showed that a minimum coherence decay and uncertainty rise occurred for $\Delta_z = 3.5$ when compared to $\Delta_z = 1.0$. The entanglement and coherence functions stayed in inverse relation with the entropic uncertainty/entropy functions; as can be seen, both grew in opposite directions.

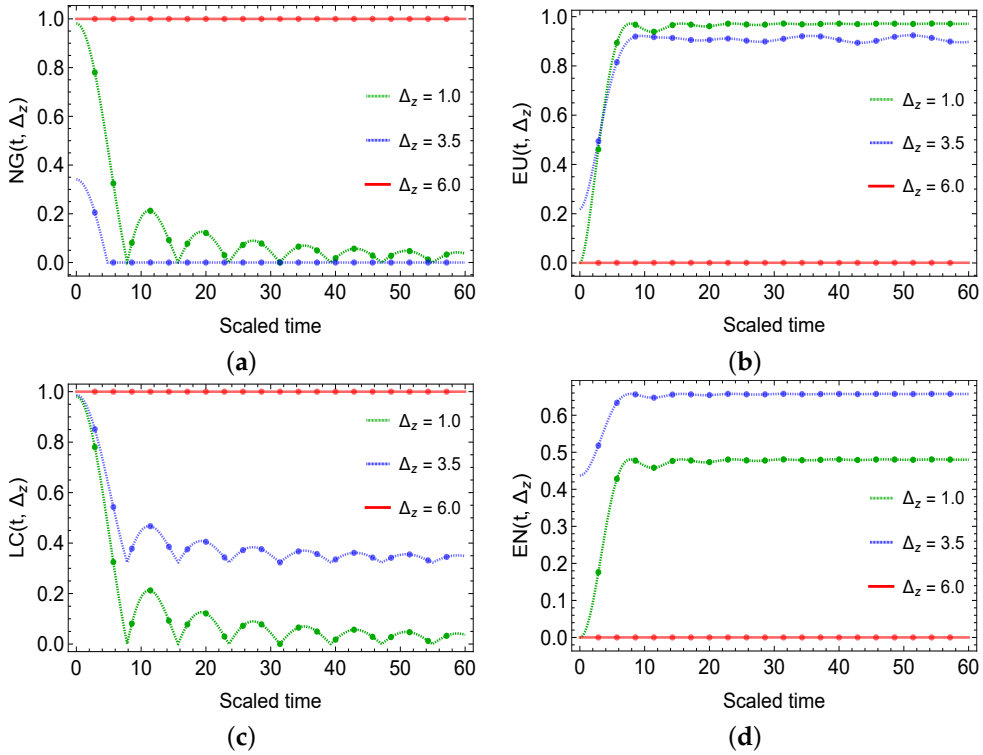

Figure 8. Dynamics of negativity (**a**), entropic uncertainty (**b**), ℓ_1-norm coherence (**c**), and linear entropy (**d**) as functions of the symmetric exchange spin-spin interaction strength in the z-direction along Δ_z against time in a two-spin state influenced by an external TMCC. For all the plots, we set $\Delta_Q = 2$, $\lambda = 0.1$, $K_z = 5$, and $J/D_z/B/J = 1$.

In Figure 9, we investigate the impact of Heisenberg exchange interaction parameter J on the preservation of entanglement/coherence and the generation of entropic uncertainty and entropy disorder in the spin state exposed to the TMCC. We demonstrated the results for the ferromagnetic ($J < 0$), as well as for the antiferromagnetic ($J > 0$) regimes. The impact of both the ferromagnetic and antiferromagnetic regimes was found to similarly affect the generation of entanglement and the suppression of the entropic uncertainty and disorder in the state. As can be seen for both the positive and negative regimes of the Heisenberg exchange interaction, the entanglement and coherence functions were gradually generated, while the entropic uncertainty and entropy functions decayed with time. Notice that, for certain critical ranges, such as $\pm 3.5 < J < \pm 4.5$, the state seemed initially partially

entangled while having non-zero uncertainty and mixedness. Interestingly, coherence in the state was unaffected by this range, and the state remained maximally entangled and coherent. Therefore, this suggested the strengthened nature of coherence compared to the entanglement. In the range $+4.5 < J < -4.5$, the dynamics of the state exhibited either zero or partially preserved entanglement and coherence regimes at the latter intervals of time. However, for the range $\pm 4.5 < J = \pm 6.0$, the state remained maximally entangled and coherent, while encountering no decay. In agreement, for the forenamed region, the state remained completely free of uncertainty and entropy. In comparison, the coherence function exhibited a larger number of revivals of coherence compared to the other inclusive functions. As seen, all other functions exhibited a lower number of revivals or completely dissipated after a short interval of time. In one of the previous studies (Ref. [61]), for the Heisenberg spin models, the spin–spin exchange terms allowed for the state stabilization under certain conditions, which may be the actual cause for it to positively accelerate the quantum functions under certain limits.

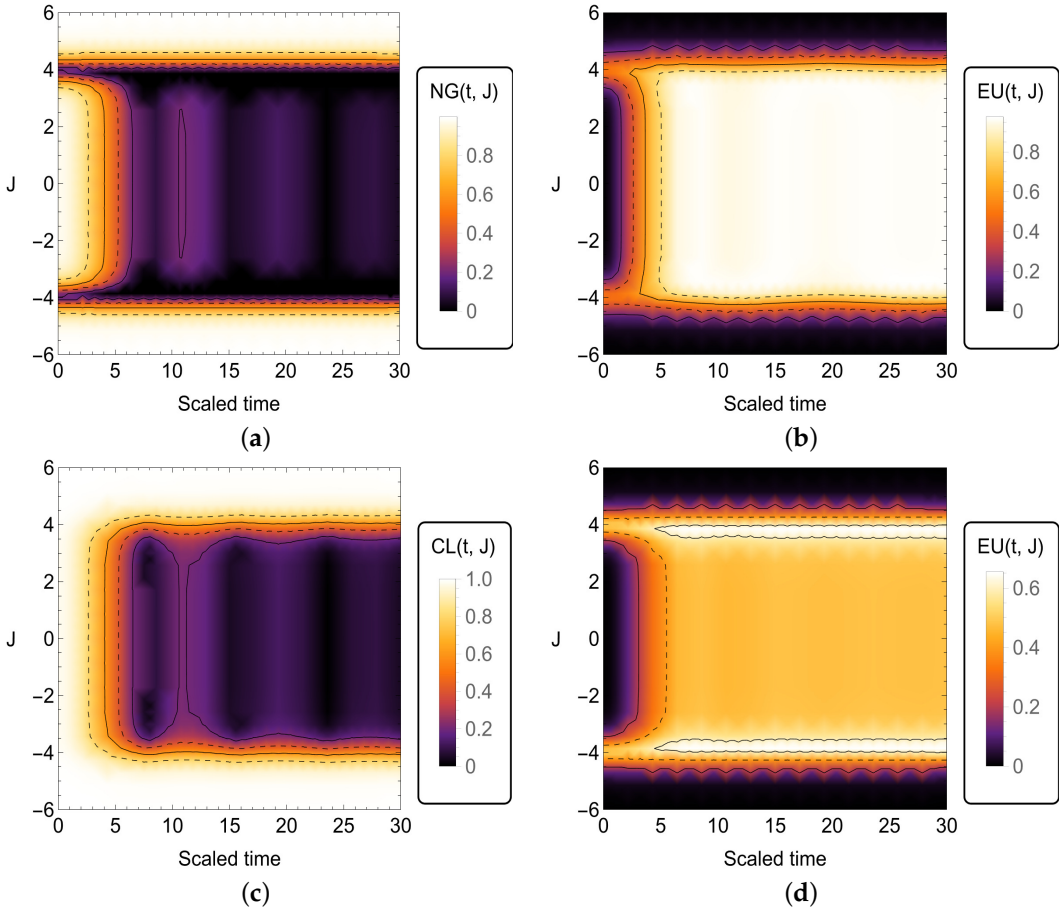

Figure 9. Dynamics of negativity (**a**), entropic uncertainty (**b**), ℓ_1-norm coherence (**c**), and linear entropy (**d**) as functions of the Heisenberg exchange interaction strength J against time in a two-spin state influenced by an external TMCC. For all the plots, we set $\Delta_Q = 2$, $\lambda = 0.1$, $K_z = 5$, $T = 0.5$ and $J/D_z/B/J = 1$.

Fidelity of the State

Finally, we give a brief account to cover how much the state becomes distinguished from the one originally assumed. In this regard, the notion of fidelity can be used to determine the discrimination between any two given states. Let one of the states be $\rho_{st}(t, T)$, given in Equation (12), and the other one be any arbitrary state σ. Further, the σ state is assumed as two categories: The first is given in Equation (5), namely $\rho(0, T)$. In the second case, let us consider a maximally entangled state $\psi = \frac{1}{\sqrt{2}}(00 + 00)$; therefore, the initial

density matrix of the state becomes $\rho_0 = \psi\psi$. Therefore, $\sigma \in \{\rho(0,T), \rho_0)\}$. Using such a comparison would lead us to clarify the distance between the resultant, initial thermal, or maximally entangled two-qubit state. In this case, the fidelity for the two matrices $\rho_{st}(t,T)$ and σ can be written as

$$FID_X = Tr[\rho_{st}(t,T)\sigma] + 2\sqrt{\det[\rho_{st}(t,T)]\det[\sigma]}, \tag{18}$$

where the fidelity between states $\rho_{st}(t,T)$ and $\rho(0,T)$ becomes

$$FID_1 = X1 + X2 + X3 \tag{19}$$

where

$$X1 = \rho_{11}^2 + \rho_{22}^2 + \rho_{33}^2 + \rho_{44}^2 + 2\rho_{23}\rho_{23}^*,$$
$$X2 = \frac{\rho_{14}\rho_{14}^* \sin(2\Delta_Q\lambda t)\cos(4\Delta_o\lambda t)}{\Delta_Q\lambda t},$$
$$X3 = \sqrt{\frac{(|\rho_{14}|^2 - \rho_{11}\rho_{44})(\rho_{22}\rho_{33} - \rho_{23}\rho_{23}^*)^2\left(\rho_{14}\rho_{14}^*\sin^2(2\Delta_Q\lambda t) - 4\Delta_Q^2\lambda^2\rho_{11}\rho_{44}t^2\right)}{\Delta_Q^2\lambda^2t^2}}.$$

Besides, the fidelity between $\rho_{st}(t,T)$ and the maximally entangled state has the form:

$$FID_2 = \frac{1}{4}\left(2(\rho_{11}+\rho_{44}) + \frac{e^{-4i\Delta_o\lambda t}\sin(2\Delta_Q\lambda t)(\rho_{14} + \rho_{14}^* e^{8i\Delta_o\lambda t})}{\Delta_Q\lambda t}\right) \tag{20}$$

In Figure 10, the fidelity dynamics for between the states $\rho_{st}(t,T) - \rho(0,T)$ (FID_1) and $\rho_{st}(t,T) - \rho_0$ (FID_2) is presented against various static noisy dephasing parameters. This would enable us to predict how much the resultant state deviates from the originally considered state under strong and weak dephasing limits. In Figure 10a, the two states seem completely comparable; however, with time, they become distinguished more and more. However, the fidelity loss rate is mostly concentrated on the dephasing strength introduced in the system. For example, for $\Delta_Q = 5.0$, the fidelity loss rate is quick enough, and so, the opposite can be seen at the weak dephasing limits. However, for the weak dephasing limits, the minimum achieved by the green slopes was deeper than that seen for the strong dephasing limits. This shows that the states became more distinguishable at a specific duration. Besides, for the stronger dephasing strengths, the slopes show quicker revivals as compared to that at the weak dephasing end. After a long time, all the slopes finally seem to achieve a similar saturation level, hence predicting a similar amount of fidelity even for the different Δ_Q values. In the second case in Figure 10b, initially, the state remained more distinguishable; however, the fidelity increased between the states $\rho_{st}(t,T)$ and ρ_0. The rate of fidelity increase remained higher for the weak dephasing strengths and decreased for the higher dephasing strengths. However, with time, the slopes for the different values of Δ_Q seem to accumulate the same saturation level. This showed that there would remain a constant amount of distinguishability between the maximally entangled and our considered state $\rho_{st}(t,T)$ in the current given conditions.

Furthermore, in the current work, we found that entropic uncertainty and entropic disorder negatively affect the degree of quantum correlations in the state. As can be seen, when the entropic uncertainty and disorder rose, entanglement and coherence decayed. It is noticeable that the rate of entropic uncertainty and mixedness remained higher than the decay rate of entanglement and coherence. This suggested that the entropic uncertainty and disorder in the two-qubit spin states led, while the oppositefunctions lagged, hence illustrating the rise in uncertainty and entropy as the major causes of the loss of quantum correlations in the spin systems. Besides, we believe that the current configuration can be successfully employed for the transmission of quantum information in

associated protocols. As can be seen, this configuration can be readily exploitable to induce longer quantum correlation preservation. Moreover, the cases of the implementation of individual classical channels have been found to be damaging to the quantum correlation preservation compared to when the classical channel is employed jointly with an external magnetic field [8,45]. In addition, the current results also show that the same configuration with individual external magnetic fields and thermal fields exhibits lesser and shorter preserved quantum correlations compared to when it is jointly employed with the classical field [32,56,57].

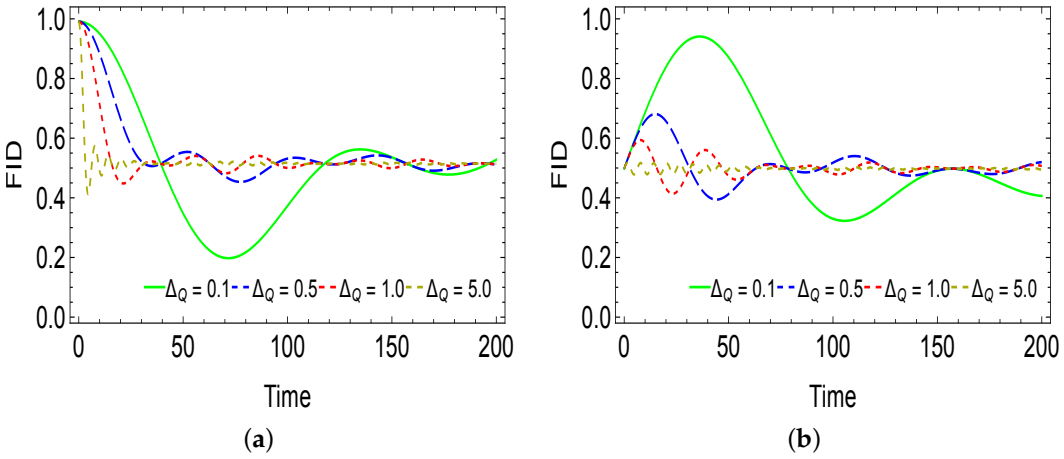

Figure 10. (**a**) Dynamics of fidelity between states $\rho_{st}(t,T)$ and $\rho(0,T)$ for the two-qubit case when exposed to the hybrid channel against various strengths of classical dephasing while setting $\lambda = 0.1$, $K_z = 5$, $T = 0.5$, and $J/D_z/B/J = 1$. (**b**) Same as (**a**), but for $\rho_{st}(t,T)$ and ρ_0.

4. Experimental Feasibility

Any configuration, without its experimental nature, would be assumed not to be beneficial. For this reason, we give some experimental prospects for the current studied configuration. We found that classical channels have been experimentally well adopted with quantum channels previously for information processing; for example, see Refs. [62–65]. In Ref. [62], by keeping a spacing of 1.6nm between the local and non-local channels while tuning the frequency to 200 GHz at -24 dBm, the authors disclosed a resourceful joint channel. They found the total coexistence power in single-mode fiber (SMF), where the secret key rate (SKR) was recorded to drop by 73%. Besides this, at 0 dBm, for the total coexistence power in hollow core nested antiresonant nodeless (HC-NAN) fiber (250-times greater power savings than that achieved for SMF), the SKR remained more preserved. The co-deployment of a discrete variable–quantum key distribution channel with 8×200 Gbps classical channels was resourcefully demonstrated using a 2 km-long HC-NAN fiber with a high-speed transmission of 1.6 Tbps [63]. Here, the authors claimed the coexistence of classical–quantum channels was recorder to have a reduced decay and even more power savings (nearly 40-times) compared to the individual utilization of quantum channels. In reference to our study, the authors in Ref. [64] experimentally probed the counter-propagation of local quantum channels over a 1km-long seven-core, multicore fiber and found that they showed high tolerance to the noise compared to the individual use of the counterparts, hence showing agreement with our results. The authors in Ref. [65] realized a quantum–classical channel over a seven-core multicore fiber, based on space division multiplexing with the highest launch power of 25 dBm. By looking into the above studies, it can be readily deduced that classical channels can be combined together with quantum channels such as the ones studied here. Moreover, we proposed that, if the current configuration is utilized by applying certain procedures, then it might turn out to be a resourceful way for the practical transmission of quantum information, quantum devices, and associated quantum operations.

5. Conclusions

This study disclosed the characterization of a hybrid channel comprising thermal, magnetic, and classical parts characterized by various quantum correlations' strengthening and weakening characteristics. The case of a two-qubit state for the sake of simplicity was introduced to investigate the time evolution of entanglement, coherence, entropic uncertainty, and entropy disorder under the considered channel. Various quantum tools were used to characterize the parameters of the configuration, and the resultant dynamical maps of the assumed quantum criteria were explicitly studied. Finally, we provided the optimal parameter setting that best suited quantum correlation preservation and entropic uncertainty, as well as disorder suppression under the action of the hybrid channel.

We demonstrated that the collective symmetry of the current configuration shared by the thermal, magnetic, and classical fields continues to be a crucial factor in maintaining the preservation of quantum correlations. There exist certain aspects in this joint external field setup that can be used to avoid the emergence of entropic uncertainty and entropy disorder in the state. For example, in the weaker coupling regimes of the classical field, for certain values of the DM, spin–spin, and anisotropy interaction strengths, the state remains maximally entangled and coherent initially, as well as for the latter interval of time. In close connection, for the given conditions, the state can be kept completely free of uncertainty and entropy disorder. The entanglement and coherence decay were found to completely depend on the emergence of the entropic uncertainty and entropy disorder in the two-qubit spin state system. Certain aspects of the coupled fields, such as the coupling strengths, the disorder parameter of the static noise, the magnetic field strength, and the temperature of the hybrid channel were found to be responsible for the emergence of the uncertainty and entropy, as well as for the decay of the entanglement and coherence. Interestingly, previously, the KSEA interaction was found to be highly influential for the preservation of quantum correlations; however, the opposite was witnessed when imposed with the current hybrid channel. Finally, we believe that the intersection of the thermal, classical, and magnetic fields along with certain state parameters remains a vital choice, which shows the capacity to be controlled easily for the preservation of quantum data compared to that when they are considered individually.

Author Contributions: Conceptualization, A.u.R. and C.Q.; Methodology, A.u.R. and C.Q.; Software, A.u.R.; Validation, A.u.R., C.Q. and M.Y. Formal Analysis, C.Q.; Investigation, A.u.R.; Resources, A.u.R. and C.Q.; Data Curation, C.Q. and S.M.Z.; Writing—Original Draft Preparation, A.u.R. and S.M.Z.; Writing—Review and Editing, A.u.R., M.Y. and C.Q.; Visualization, A.u.R.; Supervision, C.Q.; Project Administration, C.Q.; Funding Acquisition, C.Q. All authors have read and agreed to the published version of the manuscript.

Funding: This work was supported in part by the National Natural Science Foundation of China (NSFC) under Grants 11975236 and 12235008 and by the University of Chinese Academy of Sciences.

Data Availability Statement: Data are contained within the article.

Conflicts of Interest: The authors declare no conflict of interest.

References

1. Coecke, B.; Heunen, C.; Kissinger, A. Categories of quantum and classical channels. *Quantum Inf. Process.* **2016**, *15*, 5179–5209. [CrossRef]
2. Dahbi, Z.; Rahman, A.U.; Mansour, M. Skew information correlations and local quantum Fisher information in two gravitational cat states. *Phys. A Stat. Mech. Its Appl.* **2023**, *609*, 128333. [CrossRef]
3. Dahbi, Z.; Oumennana, M.; Anouz, K.E.; Mansour, M.; Allati, A.E. Quantum Fisher information versus quantum skew information in double quantum dots with Rashba interaction. *Appl. Phys. B* **2023**, *129*, 27. [CrossRef]
4. Nweke, N.I.; Toliver, P.; Runser, R.J.; McNown, S.R.; Khurgin, J.B.; Chapuran, T.E.; Dallmann, N. Experimental characterization of the separation between wavelength-multiplexed quantum and classical communication channels. *Appl. Phys. Lett.* **2005**, *87*, 174103. [CrossRef]
5. Hosur, P.; Qi, X.L.; Roberts, D.A.; Yoshida, B. Chaos in quantum channels. *J. High Energy Phys.* **2016**, *2016*, 4. [CrossRef]
6. Khanna, V.K. Short-channel effects in MOSFETs. In *Integrated Nanoelectronics*; Springer: New Delhi, India 2016; pp. 73–93.

7. Neuber, A.; Butcher, M.; Hatfield, L.L.; Krompholz, H. Electric current in dc surface flashover in vacuum. *J. Appl. Phys.* **1999**, *85*, 3084–3091. [CrossRef]
8. Rahman, A.U.; Noman, M.; Javed, M.; Ullah, A.; Luo, M.X. Effects of classical fluctuating environments on decoherence and bipartite quantum correlations dynamics. *Laser Phys.* **2021**, *31*, 115202. [CrossRef]
9. Lami, L. Non-classical correlations in quantum mechanics and beyond. *arXiv* **2018**, arXiv:1803.02902.
10. Horodecki, R.; Horodecki, P.; Horodecki, M.; Horodecki, K. Quantum entanglement. *Rev. Mod. Phys.* **2009**, *81*, 865. [CrossRef]
11. Steane, A. Quantum computing. *Rep. Prog. Phys.* **1998**, *61*, 117. [CrossRef]
12. Chen, X.B.; Wang, T.Y.; Du, J.Z.; Wen, Q.Y.; Zhu, F.C. Controlled quantum secure direct communication with quantum encryption. *Int. J. Quantum Inf.* **2008**, *6*, 543–551. [CrossRef]
13. Gottesman, D.; Jennewein, T.; Croke, S. Longer-baseline telescopes using quantum repeaters. *Phys. Rev. Lett.* **2012**, *109*, 070503. [CrossRef] [PubMed]
14. Degen, C.L.; Reinhard, F.; Cappellaro, P. Quantum sensing. *Rev. Mod. Phys.* **2017**, *89*, 035002. [CrossRef]
15. Guy, D.C. *The Weaponization of Quantum Physics: How Technology Is Transforming Warfare*; Gravely Naval Research Group, Naval War College: Newport, Rhode Island, 2018.
16. Remy, M.; Bokic, B.; Cormann, M.; Kubo, W.; Caudano, Y.; Kolaric, B. Transmission of entangled photons studied by quantum tomography: Do we need plasmonic resonances? *J. Phys. Commun.* **2019**, *3*, 065011. [CrossRef]
17. Abd-Rabbou, M.Y.; Khalil, E.M.; Al-Awfi, S. *Noise-Based Damping of Chaotic Entanglement in Pulsed Driven Two-Qubit System*; Annalen der Physik; Wiley: Hoboken, NJ, USA, 2023; p. 2300423.
18. Abd-Rabbou, M.Y.; Metwally, N.; Ahmed, M.M.A.; Obada, A.S. Suppressing the information losses of accelerated qubit–qutrit system. *Int. J. Quantum Inf.* **2019**, *17*, 1950032. [CrossRef]
19. Wu, K.D.; Streltsov, A.; Regula, B.; Xiang, G.Y.; Li, C.F.; Guo, G.C. Experimental progress on quantum coherence: Detection, quantification, and manipulation. *Adv. Quantum Technol.* **2021**, *4*, 2100040. [CrossRef]
20. Cassidy, D.C. Heisenberg, uncertainty and the quantum revolution. *Sci. Am.* **1992**, *266*, 106–113. [CrossRef]
21. Oppenheim, J.; Wehner, S. The uncertainty principle determines the nonlocality of quantum mechanics. *Science* **2010**, *330*, 1072–1074. [CrossRef]
22. Kennard, E.H. Zur quantenmechanik einfacher bewegungstypen. *Z. FüR Phys.* **1927**, *44*, 326–352. [CrossRef]
23. Deutsch, D. Uncertainty in quantum measurements. *Phys. Rev. Lett.* **1983**, *50*, 631. [CrossRef]
24. Kraus, K. Complementary observables and uncertainty relations. *Phys. Rev. D* **1987**, *35*, 3070. [CrossRef]
25. Maassen, H.; Uffink, J.B. Generalized entropic uncertainty relations. *Phys. Rev. Lett.* **1988**, *60*, 1103. [CrossRef]
26. Ming, F.; Wang, D.; Fan, X.G.; Shi, W.N.; Ye, L.; Chen, J.L. Improved tripartite uncertainty relation with quantum memory. *Phys. Rev. A* **2020**, *102*, 012206. [CrossRef]
27. Wang, D.; Ming, F.; Song, X.K.; Ye, L.; Chen, J.L. Entropic uncertainty relation in neutrino oscillations. *Eur. Phys. J. C* **2020**, *80*, 800. [CrossRef]
28. Wu, L.; Ye, L.; Wang, D. Tighter generalized entropic uncertainty relations in multipartite systems. *Phys. Rev. A* **2022**, *106*, 062219. [CrossRef]
29. Santos, L.F. Integrability of a disordered Heisenberg spin-1/2 chain. *J. Phys. A Math. Gen.* **2004**, *37*, 4723. [CrossRef]
30. Heisenberg, W. Zur theorie des ferromagnetismus. In *Original Scientific Papers Wissenschaftliche Originalarbeiten*; Springer: Berlin/Heidelberg, Germany, 1985; pp. 580–597.
31. Hernandez, R.; Lopez, E. The SU (3) spin chain sigma model and string theory. *J. High Energy Phys.* **2004**, *2004*, 052. [CrossRef]
32. Oumennana, M.; Rahman, A.U.; Mansour, M. Quantum coherence versus non-classical correlations in XXZ spin-chain under Dzyaloshinsky–Moriya (DM) and KSEA interactions. *Appl. Phys. B* **2022**, *128*, 162. [CrossRef]
33. Huang, Y.; Moore, J.E. Excited-state entanglement and thermal mutual information in random spin chains. *Phys. Rev. B* **2014**, *90*, 220202. [CrossRef]
34. Wang, D.; Huang, A.; Ming, F.; Sun, W.; Lu, H.; Liu, C.; Ye, L. Quantum-memory-assisted entropic uncertainty relation in a Heisenberg XYZ chain with an inhomogeneous magnetic field. *Laser Phys. Lett.* **2017**, *14*, 065203. [CrossRef]
35. Chlih, A.A.; Habiballah, N.; Nassik, M. Dynamics of quantum correlations under intrinsic decoherence in a Heisenberg spin chain model with Dzyaloshinskii–Moriya interaction. *Quantum Inf. Process.* **2021**, *20*, 92. [CrossRef]
36. Werlang, T.; Trippe, C.; Ribeiro, G.A.P.; Rigolin, G. Quantum correlations in spin chains at finite temperatures and quantum phase transitions. *Phys. Rev. Lett.* **2010**, *105*, 095702. [CrossRef] [PubMed]
37. Zheng, Y.; Mao, Z.; Zhou, B. Thermal quantum correlations of a spin-1/2 Ising–Heisenberg diamond chain with Dzyaloshinskii–Moriya interaction. *Chin. Phys. B* **2018**, *27*, 090306. [CrossRef]
38. Omri, M.; Abd-Rabbou, M.Y.; Khalil, E.M.; Abdel-Khalek, S. Thermal information and teleportation in two-qutrit Heisenberg XX chain model. *Alex. Eng. J.* **2022**, *61*, 8335–8342. [CrossRef]
39. Koretsune, T.; Kikuchi, T.; Arita, R. First-principles evaluation of the Dzyaloshinskii–Moriya interaction. *J. Phys. Soc. Jpn.* **2018**, *87*, 041011. [CrossRef]
40. Zheludev, A.; Maslov, S.; Tsukada, I.; Zaliznyak, I.; Regnault, L.P.; Masuda, T.; Shirane, G. Experimental Evidence for Kaplan–Shekhtman–Entin-Wohlman–Aharony Interactions in $Ba_2CuGe_2O_7$. *Phys. Rev. Lett.* **1998**, *81*, 5410. [CrossRef]
41. Wang, D.W.; Song, C.; Feng, W.; Cai, H.; Xu, D.; Deng, H.; Scully, M.O. Synthesis of antisymmetric spin exchange interaction and chiral spin clusters in superconducting circuits. *Nat. Phys.* **2019**, *15*, 382–386. [CrossRef]

42. Miranowicz, A.; Grudka, A. Ordering two-qubit states with concurrence and negativity. *Phys. Rev. A* **2004**, *70*, 032326. [CrossRef]
43. Baumgratz, T.; Cramer, M.; Plenio, M.B. Quantifying coherence. *Phys. Rev. Lett.* **2014**, *113*, 140401. [CrossRef]
44. Hu, M.L.; Fan, H. Upper bound and shareability of quantum discord based on entropic uncertainty relations. *Phys. Rev. A* **2013**, *88*, 014105. [CrossRef]
45. Rahman, A.U.; Khedif, Y.; Javed, M.; Ali, H.; Daoud, M. Characterizing Two-Qubit Non-Classical Correlations and Non-Locality in Mixed Local Dephasing Noisy Channels. *Ann. Phys.* **2022**, *534*, 2200197. [CrossRef]
46. Tchoffo, M.; Kenfack, L.T.; Fouokeng, G.C.; Fai, L.C. Quantum correlations dynamics and decoherence of a three-qubit system subject to classical environmental noise. *Eur. Phys. J. Plus* **2016**, *131*, 380. [CrossRef]
47. Glässl, M.; Croitoru, M.D.; Vagov, A.; Axt, V.M.; Kuhn, T. Influence of the pulse shape and the dot size on the decay and reappearance of Rabi rotations in laser driven quantum dots. *Phys. Rev. B* **2011**, *84*, 125304. [CrossRef]
48. Vagov, A.; Glässl, M.; Croitoru, M.D.; Axt, V.M.; Kuhn, T. Competition between pure dephasing and photon losses in the dynamics of a dot-cavity system. *Phys. Rev. B* **2014**, *90*, 075309. [CrossRef]
49. Vidal, G.; Werner, R.F. Computable measure of entanglement. *Phys. Rev. A* **2002**, *65*, 032314. [CrossRef]
50. Renes, J.M.; Boileau, J.C. Conjectured strong complementary information tradeoff. *Phys. Rev. Lett.* **2009**, *103*, 020402. [CrossRef]
51. Berta, M.; Christandl, M.; Colbeck, R.; Renes, J.M.; Renner, R. The uncertainty principle in the presence of quantum memory. *Nat. Phys.* **2010**, *6*, 659. [CrossRef]
52. Rana, S.; Parashar, P.; Lewenstein, M. Trace-distance measure of coherence. *Phys. Rev. A* **2016**, *93*, 012110. [CrossRef]
53. Neverov, V.D.; Lukyanov, A.E.; Krasavin, A.V.; Vagov, A.; Croitoru, M.D. Correlated disorder as a way towards robust superconductivity. *Commun. Phys.* **2022**, *5*, 177. [CrossRef]
54. Kropf, C.M. Protecting quantum coherences from static noise and disorder. *Phys. Rev. Res.* **2020**, *2*, 033311. [CrossRef]
55. Jiang, J.J.; Liu, Y.J.; Tang, F.; Yang, C.H. Quantum correlations in the dimerized spin chain at zero and finite temperatures. *Eur. Phys. J. B* **2011**, *81*, 419–424. [CrossRef]
56. Hashem, M.; Mohamed, A.B.A.; Haddadi, S.; Khedif, Y.; Pourkarimi, M.R.; Daoud, M. Bell nonlocality, entanglement, and entropic uncertainty in a Heisenberg model under intrinsic decoherence: DM and KSEA interplay effects. *Appl. Phys. B* **2022**, *128*, 87. [CrossRef]
57. Youssef, M.; Ali, S.I.; Abd-Rabbou, M.Y.; Obada, A.S. Exploring quantum correlations of two-qubit Heisenberg chain model influenced by magnetic dipole–dipole, magnetic field, and a symmetric cross interaction. *Quantum Inf. Process.* **2023**, *22*, 229. [CrossRef]
58. Mühlbauer, S.; Gvasaliya, S.; Ressouche, E.; Pomjakushina, E.; Zheludev, A. Phase diagram of the Dzyaloshinskii-Moriya helimagnet Ba 2 CuGe 2 O 7 in canted magnetic fields. *Phys. Rev. B* **2012**, *86*, 024417. [CrossRef]
59. Werlang, T.; Rigolin, G. Thermal and magnetic quantum discord in Heisenberg models. *Phys. Rev. A* **2010**, *81*, 044101. [CrossRef]
60. Kargarian, M.; Jafari, R.; Langari, A. Dzyaloshinskii-Moriya interaction and anisotropy effects on the entanglement of the Heisenberg model. *Phys. Rev. A* **2009**, *79*, 042319. [CrossRef]
61. Yamaji, Y.; Nomura, Y.; Kurita, M.; Arita, R.; Imada, M. First-principles study of the honeycomb-lattice iridates Na_2IrO_3 in the presence of strong spin-orbit interaction and electron correlations. *Phys. Rev. Lett.* **2014**, *113*, 107201. [CrossRef] [PubMed]
62. Alia, O.; Tessinari, R.S.; Bahrani, S.; Bradley, T.D.; Sakr, H.; Harrington, K.; Simeonidou, D. Dv-qkd coexistence with 1.6 tbps classical channels over hollow core fibre. *J. Light. Technol.* **2022**, *40*, 5522–5529. [CrossRef]
63. Alia, O.; Tessinari, R.S.; Bradley, T.D.; Sakr, H.; Harrington, K.; Hayes, J.; Simeonidou, D. 1.6 tbps classical channel coexistence with dv-qkd over hollow core nested antiresonant nodeless fibre (hc-nanf). In Proceedings of the 2021 European Conference on Optical Communication, Bordeaux, France, 13–16 September 2021.
64. Hugues-Salas, E.; Alia, O.; Wang, R.; Rajkumar, K.; Kanellos, G.T.; Nejabati, R.; Simeonidou, D. 11.2 tb/s classical channel coexistence with dv-qkd over a 7-core multicore fiber. *J. Light. Technol.* **2020**, *38*, 5064–5070. [CrossRef]
65. Geng, J.Q.; Fan-Yuan, G.J.; Li, K.J.; Tang, M.; Wang, S.; He, D.Y.; Han, Z.F. Integration in the C-band between quantum key distribution and the classical channel of 25 dBm launch power over multicore fiber media. *Opt. Lett.* **2022**, *47*, 3111–3114. [CrossRef]